Three dimensional imaging of damage in structural materials using high resolution micro-tomography

Jean-Yves Buffiere, Henry Proudhon, Emilie Ferrie, Wolfgang Ludwig, Eric Maire, Peter Cloetens

Three dimensional imaging of damage in structural materials using high resolution micro-tomography

J.-Y. Buffière [a,*], H. Proudhon [a], E. Ferrie [a], W. Ludwig [a], E. Maire [a], P. Cloetens [b]

[a] *GEMPPM UMR CNRS 5510, INSA Lyon, 20 Av. A. Einstein, 69621 Villeurbanne Cedex, France*
[b] *ESRF Grenoble, France*

This paper presents recent results showing the ability of high resolution synchrotron X-ray micro-tomography to image damage initiation and development during mechanical loading of structural metallic materials. First, the initia-tion, growth and coalescence of porosities in the bulk of two metal matrix composites have been imaged at different stages of a tensile test. Quantitative data on damage development has been obtained and related to the nature of the composite matrix. Second, three dimensional images of fatigue crack have been obtained in situ for two different Al alloys submitted to fretting and/or uniaxial in situ fatigue. The analysis of those images shows the strong interaction of the cracks with the local microstructure and provides unique experimental data for modelling the behaviour of such short cracks.

Keywor ds: Damage; Fatigue; Short cracks; Micro-tomography

1. Introduction

In the field of structural materials, lifetime prediction is a key issue with important economical and social impacts. Indeed, reliable predictions of durability enable a more precise design of components and therefore help reduce manufacturing costs; failure prediction can also save human lives. However, making predictions for the life of a mechanical component is quite a difficult task. It requires a detailed characterisation of the microscopic damage mechanisms leading to failure during strain/stress application. This problem is rendered more complex by the fact that very different mechanisms can be activated

* Corresponding author. Tel./fax: +33 72438854.
E-mail address: jean-yves.buffiere@insa-lyon.fr (J.-Y. Buffière).

depending on the conditions of loading and/or on the material environment.

In spite of this complexity, all damage mechanisms result, at some stage, in the creation of new surfaces in the material. Consequently, a large amount of work carried out in the field of damage assessment consists in the characterisation of the development of those surfaces during the material lifetime.

For such a characterisation, X-ray tomography is a very attractive technique which enables the visualisation of internal features in a sample. Being a non destructive technique, it also enables, in principle, in situ visualisation of damage during loading and provides therefore the chronology of damage initiation and growth. In spite of all these advantages, this technique has been rarely used in materials science mainly because its resolution (typically around 100 μm for classical medical applications) was of limited efficiency in terms of damage characterisation. In the last ten years, however, significant progress have been made in terms of resolution with both the availability of new third generation synchrotron X-ray sources as well as new detectors [1]. Spatial resolution close to that of an optical microscope can now be achieved which opens (or re-opens) wide areas of research.

In this paper we present some recent experiments which illustrate the potential of high resolution X-ray micro-tomography for the characterisation of damage development in metallic materials under load. These experiments have all been carried out at ESRF on beamline ID19. Damage initiation and growth has been investigated in metallic alloys submitted to various type of loading conditions. In each case quantitative data can be extracted from the three-dimensional (3D) images and used to test/validate damage models.

2. Materials and experiments

2.1. Monotonic loading

The material used for the study of damage during monotonic straining is a model Al-based metal matrix composite reinforced by spherical zirconia based particles with a size ranging between 40 and 60 μm (4% volume fraction). The nature of the hard and brittle reinforcements has been selected to produce good X-ray attenuation contrast as well as good "mechanical contrast" with the ductile and low attenuating Al matrix. The spherical shape of the particles is also chosen in order to ease eventual modelling of the deformation by finite elements (FE) methods. In order to study the influence of the matrix straining rate on damage, two different matrix have been used: pure aluminium[1] and a 2124 alloy[2]. Hereafter, these materials will be named Al + 4% ZS and Al2124(T6) + 4% ZS, respectively. Their fabrication technique, based on powder metallurgy is described in detail elsewhere [2]. Small double shouldered tensile samples were spark cut from the centre of extruded bars with their axis parallel to the extrusion direction. Constant strain rate tensile tests were conducted at room temperature on a tensile testing device especially designed for in situ tensile measurements during tomography [3]. For each material, several tomographic scans were performed on the same sample at increasing strain levels on beamline ID 19 at ESRF (see [4] and [5] for the details of the set-up and the experimental conditions used, respectively), the size of the isotropic voxels in the reconstructed images is 2 μm.

2.2. Cycling loading

Two types of experiments have been performed: first, the propagation of previously initiated fretting cracks (called hereafter fretting cracks) and, second, the initiation/propagation of cracks from a defect (called hereafter natural cracks) have been monitored *in situ* in small fatigue samples.

For the fretting cracks the experimental procedure is schematically presented in Fig. 1, for a detailed description of the setup see [6]. The material investigated is a 2024 T351 damage tolerant alloy [7]. Fretting wear tests are performed in order to initiate at least a small fretting crack in

[1] Strain to failure: $\epsilon_R = 50\%$ and 0.2% Yield strength: $\sigma_{0.2} = 75$ MPa.

[2] $\epsilon_R = 15\%$ and $\sigma_{0.2} = 280$ MPa.

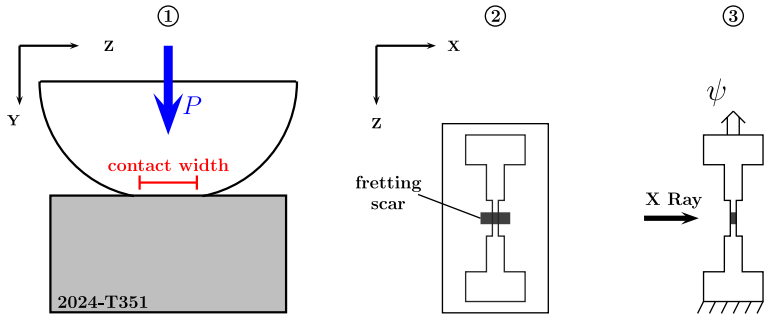

Fig. 1. Schematic illustration of the principle of the fretting crack experiment. ① Fretting cracks are induced in a piece of 2024 Al alloy using a plane/cylinder configuration ② hour glass fatigue sample are spark cut from the fretting pad ③ the fatigue samples containing the fretting crack are cycled in situ during X-ray observation in radiography and tomography.

the slip zone of the fretting scar ($N_{cycles} > 100\,000$ and $P^3 = 320$ N/mm). The test analysed in this paper corresponds to a number of applied fretting cycles of 500×10^3. Hour glass fatigue samples were obtained by electro-discharge machining of the tested fretting specimens. The tomographic setup was the same as the one reported in [8] but for the CCD detector which is a 2048×2048 pixel Frelon camera. The size of the isotropic voxels in the reconstructed images is 0.7 μm, a value which gave a good compromise between the specimen size and the spatial resolution. The specimen section to be imaged is hence restricted to 1×1 mm^2 (parallel beam). The fretting pre-cracked specimen were then loaded under fatigue thanks to a dedicated set up described in [9]. The load was applied with constant amplitude at a maximum stress of 100 MPa, with a stress ratio of 0.2 and a frequency of 5 Hz. The fatigue set up is monitored from outside the experimental hutch; several thousand fatigue cycles are applied to the specimen and a 2D radiograph of the cracked zone is recorded. When a significant change is observed on the radiographs, a tomographic scan is recorded.

For the natural cracks the experimental procedure is similar except that no crack is present in the initial state so that the initiation process is also monitored. To do so, the whole gage length of the sample (~3 mm long) was be radiographed after a given number of cycles had been performed. The material studied in that case is a cast Al alloy containing artificial pores (for a detailed description of the material see [10]). The conditions of cyclic loading are identical to those described before except for the maximal stress used: $\sigma_{Max} = 175$ MPa.

[3] Normal load defined on Fig. 1.

3. Results and analysis

3.1. Monotonic loading

Reconstructed internal sections obtained from the 3D images, are shown in Fig. 2; it can be seen on those sections (2a) that in the Al + 4%ZS composite damage occurs essentially by decohesion at particle/matrix interfaces, while reinforcement cracking is mainly observed in Al2124(T6) + 4%ZS (2b). The two composites also present respectively some particle cracking and debonding, but in lower proportion. In both materials, final fracture occurred by voids inter-linkage and percolation in the matrix of the particles micro cracks as shown on Fig. 2 [2]. A quantitative analysis of damage events has been carried out from the 3D data. The cumulative evolutions of the volume fraction of damaged particles as a function of the true plastic strain have been obtained for both materials. These fractions are calculated as the ratio of the volume of particles of each type (cracked or debonded) at each deformation stage divided by the total volume of particles accounted for in both analysis (in the considered 3D blocks). Both curves confirm the damage evolutions observed on reconstructed images. The final volume

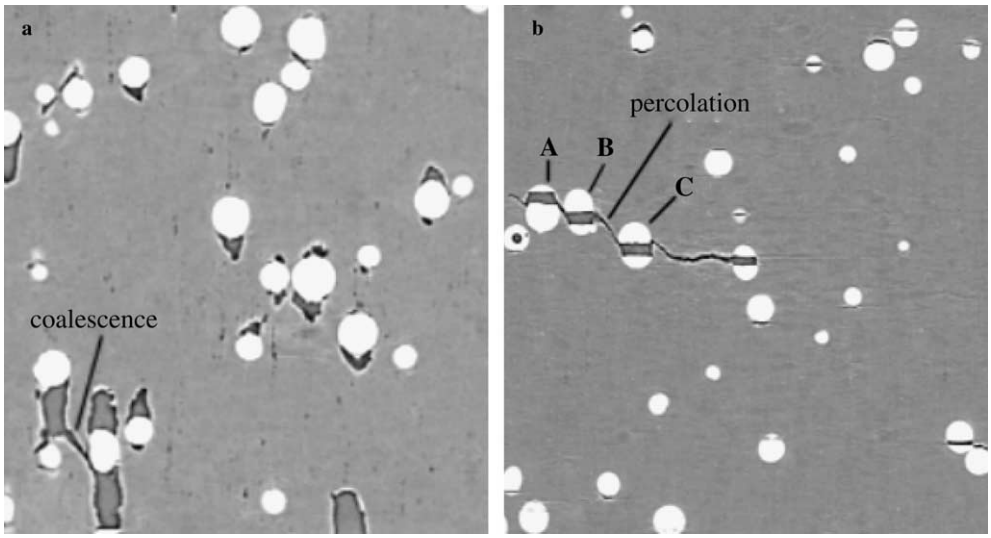

Fig. 2. Reconstructed images of the interior of the Al/ZrO_2 composites: (a) Al + 4% ZS, main damage mechanism: particle/matrix decohesion and (b) Al2124(T6) + 4% ZS, main damage mechanism: particle cracking.

fraction of cracked particle is relatively high (70%) and the damage growth rate is larger than in the case of debonded particles, leading to a more precocious global fracture of the composite Al2124(T6) + 4%ZS. The observed differences, in terms of damage events, seem to be closely linked with the different yield stresses of both matrix. Matrix softening reduces the stresses carried by the particles and the interfaces. As plastic strain increases, the load transfer from a soft matrix to the particle is not sufficient to lead to particle cracking. On the other hand, the large plastic strain undergone by the matrix cannot be accommodated by interfaces, leading to the nucleation of voids by interfacial fracture. Based on the results of damage initiation and evolution obtained in the 3D images, FE calculations were carried out in order to establish a damage criterion in the studied composites. Provided that the sources of dispersion of the local stress field in the inclusions were very weak with the model system used (good spatial distribution, narrow size range, aspect ratio close to 1), the experimentally observed scatter (in terms of plastic strain) was assumed to be due to the intrinsic rupture properties of the inclusions only. The mechanical stress field in the inclusions was assessed using simple axisymmetric FE calculations. The distribution of the fraction of damaged particles is in this case a direct picture of the scatter of the rupture strain. This distribution was assumed to follow a Weibull statistics. The Weibull properties determined for the rupture of the inclusions were satisfactory in the sense that they were identical for composites reinforced with different fraction of particles. The normal stress, the Tresca stress and the critical elastic stored energy were then validated and indirectly measured for the studied inclusions. Finally, it appeared that for the case of decohesion the different criteria investigated could not be validated [11].

3.2. Cycling loading

3.2.1. Fretting cracks

A three-dimensional rendering of the fretting crack in the initial state is presented in Fig. 3(a) which also shows (3b) one reconstructed image extracted from the interior of the material along the contact[4] in Fig. 3(a). On this figure the initiation angle θ is defined. θ is measured from the surface and for a crack extension less than 20 μm. On the slice shown in Fig. 3, the value of the local fretting crack angle is found to be: $\theta_1 = -4°$. A

[4] Detail labelled .

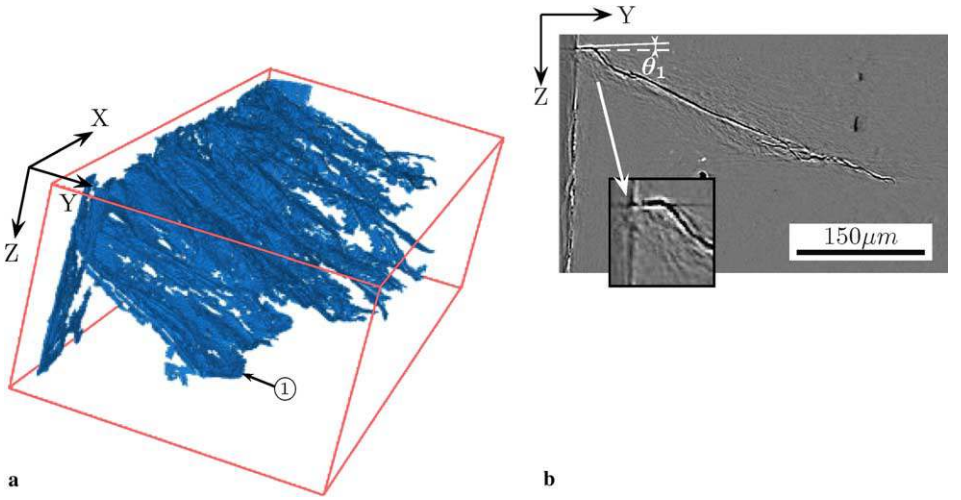

Fig. 3. Reconstructed images of a fretting crack obtained by X-ray tomography. (a) 3D rendering of the crack shape obtained by thresholding of the gray level 3D image and (b) 2D slice in the interior of the specimen showing the crack initiation angles (θ_1) at a given position along the crack front (detail ①).

systematic study of the variation of θ on the different (Y,Z) slices of the 3D image of the fretting crack is presented in Fig. 4. The curve shown on this figure reveals that the value of θ exhibits a very large scatter along the contact length (i.e. the X-axis) e.g. θ can vary from $-15°$ to $75°$. The angle between the crack plane and the surface can also be measured deeper in the material ($Y > 20$ μm) and shows a much reduced range of variation as a function of Y [7].

This result concerning the crack nucleation angle, which has never been obtained before, is very important as the value of θ is often used as one of the few relevant physical parameter for testing theoretical criterions of crack initiation under multiaxial loading. In a classical fretting experiment θ is measured on optical micrographs corresponding to cross sections of the sample parallel to the (YZ) plane. Those sections are obtained by cutting the fretting sample in two parts thus only a restricted number of θ values can be obtained with this destructive method.

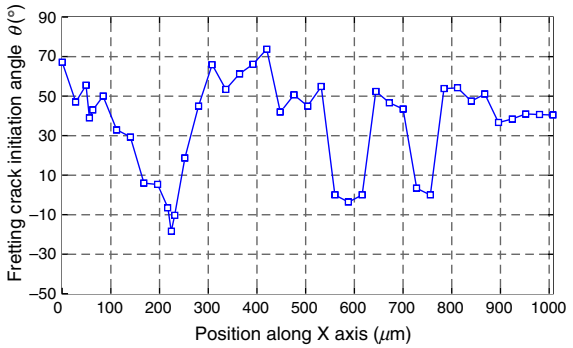

Fig. 4. Evolution along the specimen thickness of the crack initiation angle θ (as defined in Fig. 3).

At least two explanations can be suggested to account for the observed evolution of θ. The fretting crack nucleation may depend on the local microstructure, as previously observed for fatigue cracks growth in the same alloy [12]. Different crystallographic orientations along the contact length could then lead to different crack initiation angles. The curve shown on Fig. 4 exhibits some horizontal parts are likely to correspond to the crack position in one grain. This assumption is supported by the fact that the typical size of those horizontal parts is around 100 μm, which corresponds well with the grain size of the material as measured along the X direction.

A second hypothesis could be that the fretting crack nucleation is well monitored by the contact stress state. Despite the very precise contact configuration of the tests (rotation stage for alignment of the counter body, high surface qualities:

$R_a < 0.1$ μm), the crack nucleation may not be activated simultaneously all along the contact length but in distinct locations. It can be assumed that these different locations correspond to grains presenting a good orientation with respect to the maximum stress. The first cracked grains would then present a similar crack angle corresponding to the top horizontal parts in Fig. 4, i.e. 50° in this case. The successive crack propagation process should consist in linking those different crack branches by a line tension effect. This process would activate a multi orientation crack growth related to the microstructure encountered by the crack and which can explain the high scatter measured on θ angle. When all the grains are connected, the whole propagation behaviour is imposed by the contact and displays an homogeneous orientation.

When submitted to uniaxial tensile cyclic loading, the fretting crack has been observed to propagate in the material. The 3D images obtained revealed that the main crack propagation direction was steadily changing towards a mode I propagation (perpendicular to the stress axis) with more pronounced crack branching. This branching is likely to correspond to the local crack planes in the different grains. Such a behaviour is typical of a strong interaction of the crack with the local microstructure as already observed by Zhai et al. in Al–Li alloys and by Proudhon et al. in the same alloy [12] as the one studied in this work.

Further investigations are currently being carried out to determine if the variation of the local initiation angle along the X direction and/or the observed crack branching can be correlated with the presence of grain boundaries. To do so, a Gallium infiltration technique is used, which allows to image by tomography the position of internal grains boundaries in aluminium alloys [8]. With this technique, it is believed that the above mentioned hypothesis can be further tested.

3.2.2. Natural cracks

A three dimensional rendering of the crack propagation from a pore near the surface of a sample is shown in Fig. 5. The analysis of this kind of images (and of many similar ones not shown here given the limited space available) reveals important information about natural crack initiation and propagation which is summarised in what follows.

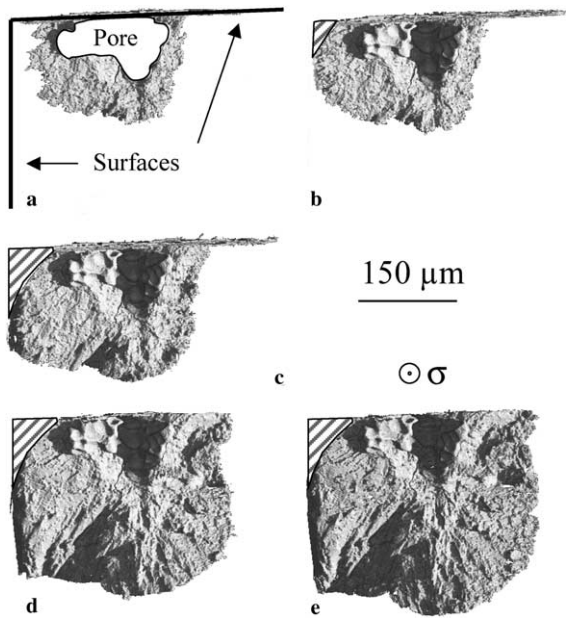

Fig. 5. Three dimensional rendering of the growth of a fatigue crack in a cast Al alloy sample cycled in situ at $\sigma_{Max} =$ 180 MPa. (a) 50 000 cycles, (b) 55 000, (c) 65 000 (d) 80 000 (e) 82 500. The hatched part of the figure in the top left corner corresponds to a cracked part of the specimen which has not been reconstructed.

Crack initiation occurs at the intersection between the pore and the surface sample; no crack initiation has been observed in the bulk of the material for the experimental conditions investigated. Such surface cracks gradually surrounds the pore which is transformed into a "bulk" crack propagating in the interior of the sample. During this surrounding phase, cracks have been observed to slow (even to stop) when grain boundaries are encountered (shown by the Ga infiltration technique). For one of the cracks studied, the number of cycles spent for transforming the pore into a crack represents 25% of the sample fatigue life. Curves giving the size a of the cracks as a function of the number of cycles N could be plotted for different positions along the crack front, corresponding to the crack propagation at the surface and in the interior of the material. It is worth mentioning that this is the first time that such experimental

curves have been directly obtained although since then similar curves have been obtained on different structural Al based or Fe based materials [13].

The curves giving the crack growth rate per fatigue cycle $\frac{da}{dN}$ as a function of the number of fatigue cycles N obtained for the cast alloy studied here show similar crack growth rate at the surface and in the bulk of the material except when a microstructural feature (pore grain boundary...) locally alters the growth rate [9]. All the cracks investigated cross a maximum of four to five grains in the small fatigue samples used (average grain size 300 μm) and are therefore far from the case of a long crack with a front encountering a hundred (or more) grains which local influence on the crack growth rate is therefore completely averaged. One might thus expect a strong effect of the local crystallography on the local growth rate of short cracks. This is a possible reason for the *short fatigue crack phenomenon* [14] observed on curves showing the evolution of $\frac{da}{dN}$ as a function of the stress intensity factor ΔK, a quantity proportional to the nominal stress σ in the sample and to the crack size a [15]. Establishing such curves at different locations along crack fronts using 3D data is however an arduous task. Semi empirical analytical expressions of the stress intensity factors can be used to account for the 3D shape of the cracks [16]. It is unlikely however that this approach can give a completely satisfactory result for the cracks studied here. Those cracks are indeed at the edge of the applicability of the linear elastic fracture mechanics because of both their small size and of the relatively high value of the cycling stress[5]. FE elasto plastic calculations of the stress intensity factors would be a better option in spite of being a much more time consuming approach. Such calculations are currently being carried out.

4. Conclusion

High resolution synchrotron X-ray microtomography has been used to investigate the initiation and development of damage in various structural metallic materials during monotonic and cycling mechanical loading. Three dimensional images of Al based metal matrix composites strained in tension have been obtained in situ. The dominant type of damage observed for these model materials depends on the matrix yield stress. Particle fracture or particle/matrix decohesions prevail when the matrix yield stress is high or low respectively. The growth rates of the two types of damage as a function of strain are found to be different. Fatigue cracks resulting from cyclic mechanical loading have been observed in two different Al alloys. The detailed quantitative analysis of a fretting crack obtained in a damage tolerant aeronautical alloy shows that fretting crack initiation is strongly correlated to the local crystallographic orientation just below the fretting pad. Further propagation in the complex stress state of the contact is found to be less sensitive to the local microstructure. The nucleation and development of natural fatigue cracks has been imaged in a cast Al–Si alloy giving the first direct evidences of the transformation of the initial defect (a pore) in a fatigue crack. This transformation is impeded by the local microstructure and can represent a non-negligible fraction of the fatigue life. In both cases, high resolution X-ray tomography appears as a very powerful novel characterisation tool for the validation and/or the development of models for the prediction of damage evolution in mechanically loaded structural materials.

[5] Chosen to give a fatigue life of approximately 8 h (one experimental shift) at a cycling frequency of 5 Hz.

References

[1] J. Baruchel, J.-Y. Buffiere, E. Maire, P. Merle, G. Peix, X-ray Tomography in Materials Science, Hermes Science Publication, Paris, 2000.

[2] L. Babout, E. Maire, J.-Y. Buffière, R. Fougères, Acta Mater. 49 (2000) 2055.

[3] J.-Y. Buffière, E. Maire, G. Lormand, R. Fougères, Acta Mater. 47 (5) (1999) 1613.

[4] P. Cloetens, M. Pateyron-Salomé, J.-Y. Buffière, G. Peix, J. Baruchel, F. Peyrin, J. Appl. Phys. D 81 (9) (1997) 5878.

[5] L. Babout, E. Maire, C. Verdu, J.-Y. Buffière, R. Fougères, in: Clyne, Simancik (Eds.), Proceedings of Euromat 99, Vol. 5, Wiley vch, 1999, p. 68.

[6] P. Kapsa, S. Fouvry, L. Vincent, Wear 200 (1996) 186.

[7] H. Proudhon, J.-Y. Buffière, S. Fouvry, in: Proceedings of ISFF4 Ecully (Fra), in press.
[8] W. Ludwig, J.Y. Buffière, S. Savelli, P. Cloetens, Acta Mater. 51 (3) (2003) 585.
[9] J.-Y. Buffiere, Mémoire d'habilitation à diriger des recherches (in French), INSA Lyon, 2002.
[10] J.-Y. Buffiere, S. Savelli, P.H. Jouneau, E. Maire, R. Fougères, Mater. Sci. Eng. A 316 (2001) 115.
[11] L. Babout, E. Maire, R. Fougères, Acta Mater. 52 (2004) 2475.
[12] H. Proudhon, J.-Y. Buffière, in: Proceedings of Fatigue Crack Path Conference Parma (It), 2004.
[13] J. Marrow, J.-Y. Buffière, P.J. Withers, G. Johnson, D. Engelberg, Int. J. Fatigue 26 (2004) 717.
[14] K.J. Miller, Fatigue Eng. Mater. Struct. 5 (3) (1982) 223.
[15] S. Suresh, Fatigue of Materials, first ed., Cambridge University Press, Cambridge, 1994.
[16] E. Ferrie, J.-Y. Buffière, W. Ludwig, in: Proceedings of Fatigue Damage of Structural Materials Hyannis Ma (USA), Sept. 2004.